Stabilization in frequency of a Laser Diode

Jean Minet
Van der Waals-Zeeman Instituut
Group of Pr. J.T.M. Walraven

August 23, 2007

Abstract

This report describes a project realized during an internship of three months at the *Van der Waals-Zeeman Instituut* of the *University of Amsterdam* for the validation of the first year of Master at the *Institut d'Optique* Graduate school in Palaiseau. This report is divided in two parts. In the first part we present the Fabry-Pérot interferometer. We discuss the basic theory of this interferometer and we describe the method we used to fix one mirror at the confocal position. In the second part, we explore different methods for locking a laser on an optical line of ^{87}Rb. We carry out a brief review of the concepts which underlie the subject and we present our locking experiment which is a kind of polarization spectroscopy based on the light-induced birefringence of our gas cell. Theoretical and experimental results are reported, the effect of magnetic field is also discussed.

Contents

Chapter 1

Introduction

Bosonic particles, which include the photon as well as atoms such as helium-4, are allowed to share quantum states with each other. Einstein speculated in 1924 that cooling bosonic atoms to a very low temperature would cause them to fall (or "condense") into the lowest accessible quantum state, resulting in a new form of matter. This transition occurs below a critical temperature T_c, which for a uniform gas consisting of non-interacting particles with no apparent internal degrees of freedom is given by:

$$T_c = \left(\frac{n}{\zeta(3/2)} \right)^{2/3} \frac{h^2}{2\pi m k_B},$$
(1.1)

where n is the particle density, m the mass per boson and ζ the Riemann zeta function ($\zeta(3/2) \simeq 2.61$).

The first BoseEinstein condensate was created by Eric Cornell, Carl Wieman, and co-workers at JILA on 1995. They did this by cooling a dilute vapor consisting of approximately 2000 rubidium-87 atoms to below 170 nK using a combination of laser cooling (a technique that won its inventors Steven Chu, Claude Cohen-Tannoudji, and William D. Phillips the 1997 Nobel Prize in Physics) and magnetic evaporative cooling. About four months later, an independent effort led by Wolfgang Ketterle at MIT created a condensate made of sodium-23. Ketterle's condensate had about a hundred times more atoms, allowing him to obtain several important results such as the observation of quantum mechanical interference between two different condensates. Cornell, Wieman and Ketterle won the 2001 Nobel Prize for their achievement.

Bose-Einstein condensate properties are still not completely understood and constitutes a very active field of research. In the *Van der Waals-Zeeman Instituut*, the group of Pr. Walraven investigate this field and is currently working on the study of exotic quantum phases of ultracold gases.

Bose-Einstein condensation is achieved with methods called Magneto-optical trapping and evaporative cooling. Magneto-optical traps (MOT) make use of optical forces in presence of a position dependent Zeeman shift. This requires to

use lasers with a frequency stabilized with respect to an atomic transition and with an accuracy below the natural linewidth ($\Gamma \simeq 6$ MHz) of the transition.

We worked first on the Fabry-Pérot interferometer, which is a nice tool to monitor the stability of laser's frequency. In a second part, we explored the different methods which can be used to lock a laser on a resonant line and realized a setup which makes use of the light-induced birefringence to lock our DFB laser.

Chapter 2

The Fabry-Pérot etalon

2.1 Introduction

The Fabry-Pérot interferometer or etalon is the most commonly used multiple beam interferometer. It is typically made of a transparent plate with two reflecting surfaces, or two parallel highly reflecting mirrors. At the origin, the two mirrors were plane, but nowadays spherical mirrors are most commonly used. Etalons are widely used in telecommunications, lasers and spectroscopy for controlling and measuring the wavelength of light. Recent advances in fabrication technique allow the creation of very precise tunable Fabry-Pérot interferometers. Fabry-Pérot interferometers also form the most common type of optical cavity used in laser construction. In this project, we made a 150 mm long scanning Fabry-Pérot interferometer in order to use it later to monitor lasers used for spectroscopy of Rubidium atom in a Bose-Einstein condensate.

2.2 Theoretical study of the Fabry-Pérot etalon

2.2.1 Principle

The principle of the Fabry-Pérot is very simple. The varying transmission function of an etalon is caused by interference between the multiple reflections of light between the two reflecting surfaces. Constructive interference occurs if the transmitted beams are in phase, and this corresponds to high-transmission peak of the etalon. If the transmitted beams are out-of-phase, destructive interference occurs and this corresponds to a transmission minimum.

2.2.2 Calculation of the transmission function

For each of the two mirrors, let r be the reflection coefficient [1], and t be the transmission coefficient. Let be $A^{(i)}$, $A^{(t)}$ and $A^{(r)}$ respectively the amplitudes

---

[1]Ratio of reflected and incident amplitudes

of the electric vector of the incident light, transmitted light and reflected light. Let be $A^{(t)}(p)$ the amplitude of the light transmitted after $2p$ reflections. Thus

$$A^{(t)}(p) = A^{(i)}t^2 r^{2p}(\exp(\frac{2i\pi L}{\lambda}))^{2p} \tag{2.1}$$

Where L is the optical length of the cavity and λ is the wavelength of the incident light [2]. The amplitude of the whole transmitted light $A^{(t)}$ is then

$$A^{(t)} = \sum_{p=0}^{\infty} A^{(i)}t^2 r^{2p}(\exp(\frac{2i\pi L}{\lambda}))^{2p} \tag{2.2}$$

This sum is nothing else than a infinite geometric series, finally

$$A^{(t)} = \frac{A^{(i)}t^2}{1 - r^2 \exp(\frac{4i\pi L}{\lambda})} \tag{2.3}$$

We can now calculate the transmitted intensity given by $I^{(t)} = A^{(t)}A^{(t)*}$:

$$I^{(t)} = \frac{I^{(i)}\mathcal{T}^2}{1 + \mathcal{R}^2 - 2\mathcal{R}\cos(\delta)} = \frac{I^{(i)}\mathcal{T}^2}{(1 - \mathcal{R})^2 + 4\mathcal{R}\sin^2(\delta/2)}, \tag{2.4}$$

where $\mathcal{R} = r^2$, $\mathcal{T} = t^2$ and $\delta = \frac{4i\pi L}{\lambda}$. We define the parameter F [12] by the formula

$$F = \frac{4\mathcal{R}}{(1 - \mathcal{R})^2}. \tag{2.5}$$

Then we can write

$$I^{(t)} = \frac{I_0}{1 + F\sin^2(\delta/2)}. \tag{2.6}$$

When $\mathcal{R}$ approaches unity so that F is large, the intensity of the transmitted light is very small except in the immediate neighborhood of the maxima. The pattern in transmitted light then consists of narrow bright fringes on an almost completely dark background (see Figure 2.1). This is why the Fabry-Pérot interferometer is very accurate in comparison with two-beams interferometers. The sharpness of the fringes is measured by their half-width which is the width between the points on either side of a maximum where the intensity has fallen to half of its maximum value. The ratio of the separation of adjacent fringes and the half-width is called the finesse $\mathcal{F}$ of the fringes.

The points where the intensity is half its maximum value are at $\delta = 2m\pi \pm \varepsilon/2$. Assuming that F is sufficiently large, ε is sufficiently small that we can write $\sin(\varepsilon/4) \simeq \varepsilon/4$ then we obtain the half width as

$$\varepsilon = \frac{4}{\sqrt{F}}, \tag{2.7}$$

---

[2]The incident light is assumed to be monochromatic
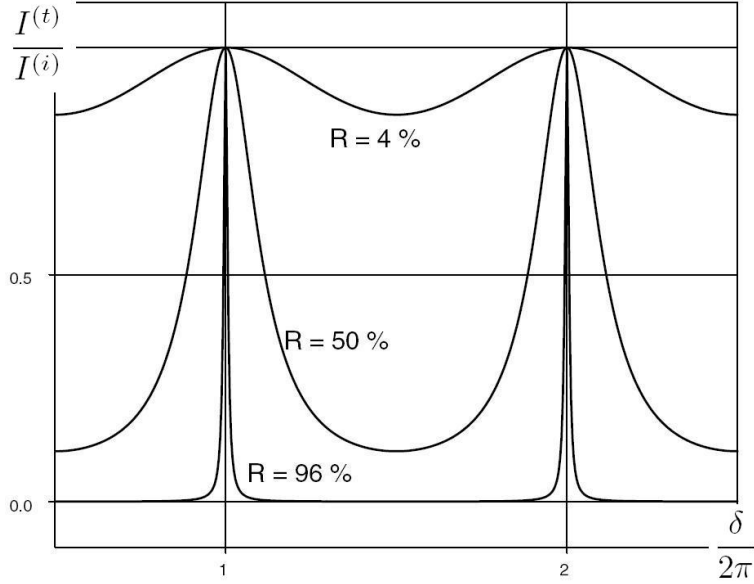
Figure 2.1: Transmission function for different reflectivities

Since the separation of adjacent fringes correspond to a change of 2π in δ, the finesse is then

$$\mathcal{F} = \frac{2\pi}{\varepsilon} = \frac{\pi\sqrt{F}}{2} = \frac{\pi\sqrt{\mathcal{R}}}{1 - \mathcal{R}}. \tag{2.8}$$

In a Fabry-Perot interferometer, the distance (in frequency space) between adjacent transmission peaks is called the free spectral range (FSR)

$$\text{FSR} = \frac{c}{2L}. \tag{2.9}$$

2.2.3 The confocal resonator

In this project, we work on a 150 mm long Fabry-Pérot resonator, which has to be setup at the confocal position as shown in Figure 2.2. It means that the length d of the resonator equals the radius of curvature R_1 and R_2 of the two mirrors. This is referred to as a confocal resonator because the focal points of the two mirrors coincide which each other at the center of the resonator. Furthermore, the confocal resonators is highly insensitive to misalignment of either mirror because tilting either mirror still leaves the center of curvature located on the other mirror surface [13]. At the surface of each mirror, the radius of curvature of the Gaussian wavefront equals the radius of curvature of the mirrors. Then we can can easily obtain the $1/e$ radial size of the beam
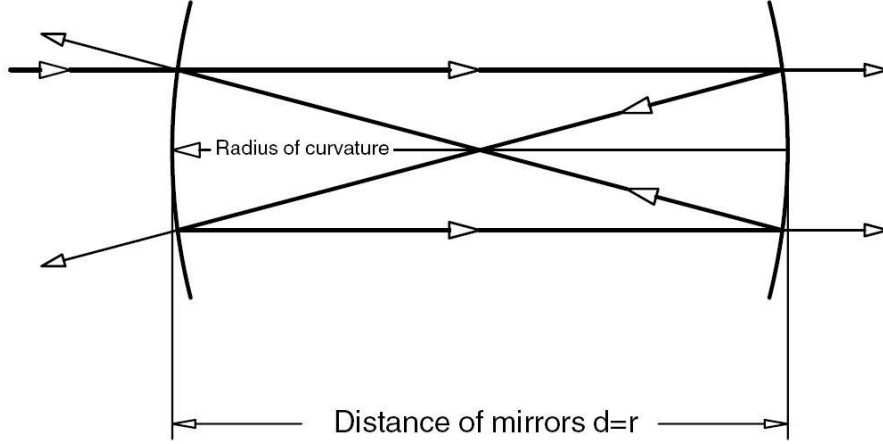
Figure 2.2: Confocal resonator

amplitude at the waist [3]:

$$w_0 = \sqrt{\frac{\lambda d}{2\pi}}. \tag{2.10}$$

Whereas the radial size is larger by $\sqrt{2}$ at the surface of the mirrors, $w = \sqrt{2}w_0$. The stability of optical resonators is discussed in Appendix A.3.

2.2.4 Gaussian transverse modes

A short introduction of the Gaussian beam is made in the Appendix A.1. Because of the Gouy phase shift [10] and its dependance on Hermite-Gaussian mode number, the different transverse modes in a stable gaussian resonator have different resonance frequencies [13]. This phenomenon induces an asymmetric broadening of the transmission peaks when the etalon is not exactly at the confocal position. For a given Hermite-Gaussian mode TEM_{mn}, the Gouy phase shift is given by (see Appendices A.1 and A.2)

$$\phi = (m + n + 1)\mathrm{Arctg}(z/z_R), \tag{2.11}$$

where z is the distance from the waist and z_R is the Rayleigh range of the Gaussian beam. Then the phase shift between the waist and either mirror is for the confocal situation [4]

$$\phi = (m + n + 1)\mathrm{Arctg}(1) = (m + n + 1)\frac{\pi}{4}. \tag{2.12}$$

---

[3] see Appendix A.1

[4] for the confocal etalon, the distance between the waist and the mirrors equals the Rayleigh range

We have finally for one round-trip

$$\phi_{\leftrightarrows} = 4\phi = (m + n + 1)\pi, \tag{2.13}$$

Which means that in the confocal position, the difference of phase for one round-trip between two consecutive even modes is 2π. Then the peaks of the even transverse modes coincide exactly with the peaks of the TEM$_{00}$ longitudinal modes. The peaks of the odd modes are placed exactly at the half-distance between two consecutive TEM$_{00}$ longitudinal modes. This results gives us a method to align the etalon (see Section 2.4. The incoming beam is a pure TEM$_{00}$ mode, then if the etalon is well aligned, the odd transverse modes cannot be excited in the cavity and we should observe the peaks due to the odd modes to be absent.

The line-shape of the transmission peaks depends on the length d of the resonator. If $d < 2Z_R$, (2.11) shows that the phase difference between two consecutive even transverse mode will be smaller than 2π. This results in a asymmetric broadening of the line-shape to the low frequency side. If $d > 2Z_R$, we will observe a broadening of the line-shape to the high frequency side. This results gives us a method to fix the input mirror at the proper longitudinal position (see Section 2.4).

2.3 Experimental setup

2.3.1 Context

The etalon is made of a 150 mm long invar [5] tube with an inner diameter of 0.5". We use two identical high reflectivity mirrors with a radius of curvature $R = 150$ mm and a diameter of 0.5". The output mirror is mounted on a piezo mount in order to scan the spectrum by varying the length of the cavity. The reflectivity of the mirrors is $R = 0.985 \pm 0.0025$, which means a theoretical finesse (2.8)

$$\mathcal{F} = 207.9 \quad (178 < \mathcal{F} < 250) \tag{2.14}$$

while the free spectral range (2.6)

$$\text{FSR} = 1 \text{ GHz}, \tag{2.15}$$

which means we expect for the FWHM of the transmission peak

$$\Delta\nu_{\text{FWHM}} = \frac{\text{FSR}}{\mathcal{F}} = 4.8 \text{ MHz}. \tag{2.16}$$

Our optical source is a frequency stabilized extended cavity diode laser which can emit light around 780 nm. The beam passes through an optical isolator to prevent feedback of light into the diode. The beam is then coupled into a

---

[5]Invar has been choosen for its very low expansion coefficient ($1.2 \cdot 10^{-6} K^{-1}$ at room temperature)
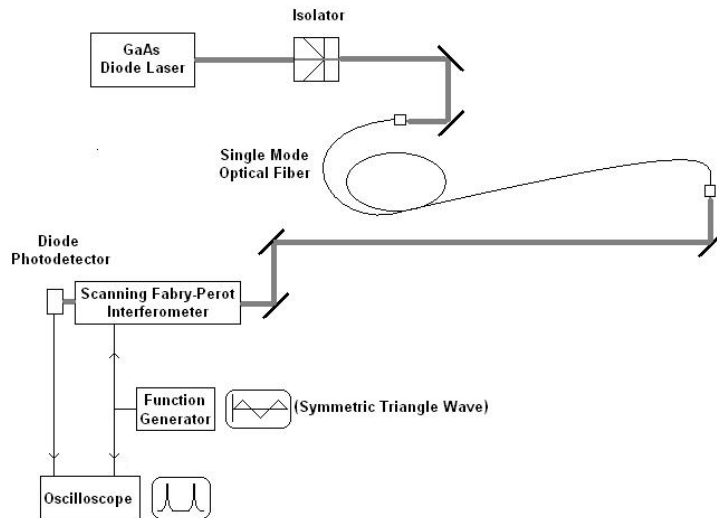
Figure 2.3: Schematic diagram of the experimental setup

single-mode fiber in order to produce a pure TEM_{00}. At the output of the fiber, the beam is collimated by a lens[6]. We use two mirrors in order to achieve proper alignment between the beam from the fiber and the etalon. At the output of the etalon, we use a photodiode connected to an oscilloscope to observe the transmission peaks when scanning the etalon with the piezo.

2.3.2   Alignment procedure

The alignment procedure involves 4 degrees of freedom : 2 degrees for the tilt and 2 degrees for the transverse position. In addition to that, we have to glue the input mirror at the proper longitudinal position.

The Fabry-Pérot etalon is considered to be well aligned and at the confocal position when the transmission peaks are perfectly symmetric [7](see Section 2.2.4) while the peaks of the odd modes are absent. When this goal is reached, we can fix the input mirror in its position with epoxy [8].

It is very difficult to get the 4 degrees of freedom decoupled. If this is the case, you only have to maximize the peaks on the oscilloscope independently for each degree of freedom. In order to get the setting of the position and the

---

[6]We measured a beam at $1/e^2$ diameter of 1.2 mm with a razor-edge mounted on a micrometer screw.

[7]The symmetry of the transmission peaks is achieved when the distance between the two mirrors equals twice the Rayleigh range

[8]We use a 8 hour drying epoxy *Stycast 1266 (Emerson & Cunning)* then we get a few time to fix the mirror in the proper position.
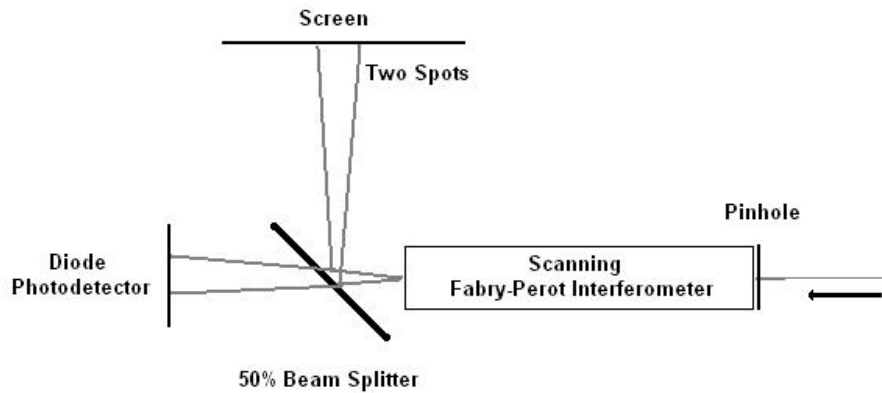
Figure 2.4: Schematic diagram of the alignment method

setting of the tilt as independent as possible, we place a mirror at 10 cm from the etalon and an other at 100 cm. We use a pinhole at the entrance of the etalon to check the position of the beam. At the exit of the etalon we observed the outcoming beam with a screen and a webcam. If the etalon is not properly aligned, we observe two spots. We only have to overlap the spots by modifying the angle of the beam to approach alignment. We reiterate this procedure until we observe a decrease of the transmission of the odd modes. Once you have observed this decrease, it is easy to make the odd modes vanish by adjusting the screws of the mirrors independently.

2.4 Experimental results

2.4.1 Characterization of the etalon

We measured the finesse of our interferometer by fitting the transmission curve with a Lorentzian as shown in Figure 2.5. The line-width of the peak is given in the plot by the parameter $w = 300$ μm, we also measure a "FSR" of 52.8 ms (which is twice the distance between the even and the odd modes shown in Figure 2.6). Then we can obtain the experimental finesse of the Fabry-Pérot

$$\mathcal{F} = \frac{\text{FSR}}{\text{FWHM}} = \frac{52.8 \text{ ms}}{300 \ \mu\text{s}} = 176 \pm 5\%. \tag{2.17}$$

We can also calculate the experimental resolution of the Fabry-Pérot

$$\Delta\nu_{\text{FWHM}} = \frac{\text{FSR}}{\mathcal{F}} = 5.7 \text{ MHz}. \tag{2.18}$$

11
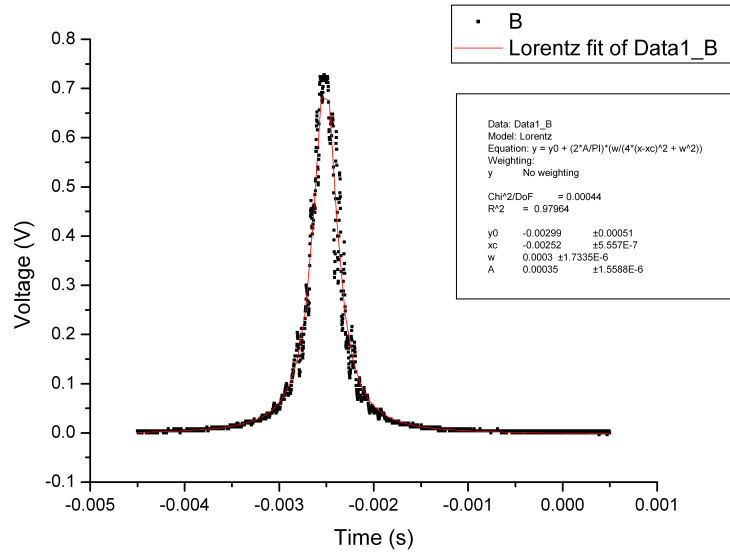
Figure 2.5: Plot of a transmission peak
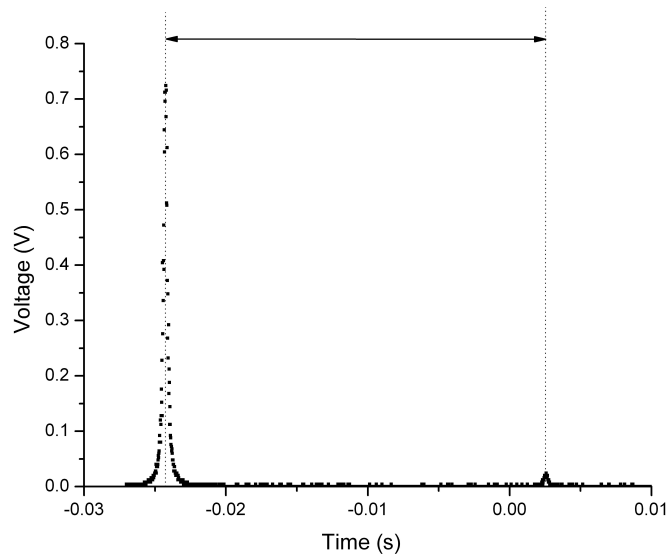
Figure 2.6: Plot of the transmission function on a half FSR

12
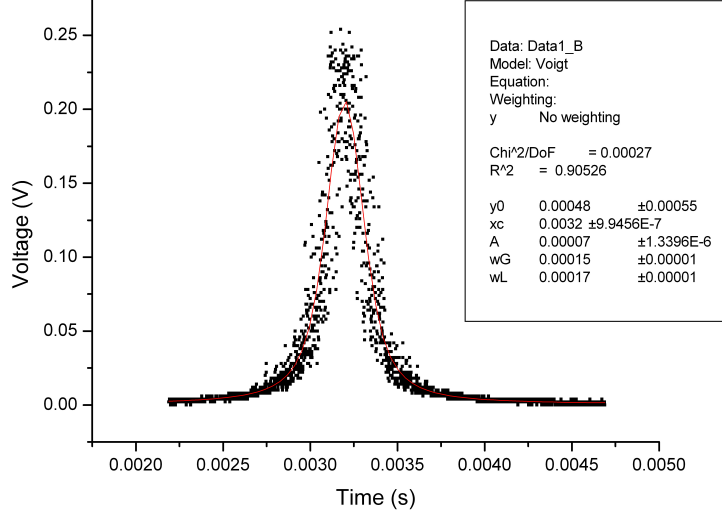
Figure 2.7: Plot of a transmission peak with the DFB Laser

2.4.2 Measurement of the band-width of a laser diode

We also tried to measure the finesse of the Fabry-Pérot using a temperature-tunable DFB laser diode as an optical source. A plot of a transmission peak is shown in Figure 2.7. The transmission peak broadens because the line-width of the DFB laser is not negligible in front of the line-width of the Fabry-Pérot. The "transmission peak" shown in Figure 2.7 is then a convolution between the spectrum of the DFB laser (which is roughly a Gaussian) and the "true" transmission peak of the etalon (which is a Lorentzian). The result of this convolution is called a Voigt profile and cannot be expressed in a simple form. However, we fit the transmission peak with a Voigt profile to obtain the Gaussian component and the Lorentzian component of the transmission peak. Then we can obtain the band-width of the laser

$$\Delta\nu_{\mathrm{G}} = \frac{\mathrm{wG}}{\Delta t_{\mathrm{FSR}}}\mathrm{FSR} = \frac{150\ \mu\mathrm{s}}{32.52\ \mathrm{ms}}.1\ \mathrm{GHz} = 4.6\ \mathrm{MHz}. \tag{2.19}$$

We can also measure the finesse of the Fabry-Pérot

$$\mathcal{F} = \frac{\Delta t_{\mathrm{FSR}}}{\mathrm{wL}} = \frac{32.52\ \mathrm{ms}}{170\ \mu\mathrm{s}} = 191, \tag{2.20}$$

which is not exactly what we expected (around 176). Although this measurement is not very accurate, we can observe that we can obtain information below the resolution of the Fabry-Pérot.

13

2.5   Concluding remarks

The experimental finesse ($\mathcal{F} = 176$) of the Fabry-Pérot is lower than expected. There are a number of causes that could explain this result:

- The reflectivity of the mirrors is lower than expected.

- The line-width of the laser is not negligible in front of the line-width of the transmission peaks.

- The roughness of the mirrors affects the finesse by scattering a small part of the light at every reflection (see discussion at Appendix A.4).

- The distance between the two mirrors does not equal exactly the radius of curvature of the two mirrors [9].

---

[9] However, this resulting asymmetric broadening can be suppressed by matching only the TEM_{00} mode into the etalon

Chapter 3

General notions of spectroscopy

We lock a laser on a optical transition of ^{87}Rb using the properties of the light transmitted through a ^{87}Rb gas-cell. We describe in this chapter the basic concepts which underlie this method. We first describe general properties of hydrogen-like atom to understand the physics behind the quantization of energy levels. In the second part, we briefly discuss the optical properties of those atoms in order to understand the modification of the laser light when passing through the gas-cell.

3.1 General properties of hydrogen-like atoms

3.1.1 Main structure

The hamiltonian of a single electron of mass m orbiting around a positively charged nucleus is given by

$$H_0 = -\frac{\hbar^2}{2m}\Delta + V(r), \tag{3.1}$$

where $V(r) = -Ze^2/4\pi\epsilon_0 r$ is the Coulomb energy. The motion of the electron can be described by a Schródinger equation of the type

$$[\frac{1}{2m}(p_r^2 + \frac{\mathbf{L}^2}{r^2}) + V(r)]\psi(r,\theta,\phi) = E\psi(r,\theta,\phi), \tag{3.2}$$

where p_r is the radial momentum operator, $\mathbf{L}$ the angular momentum operator and E the total energy of the system. Since the operators H, $\mathbf{L}^2$ and L_z commute between each other, we can find a basis of the state space composed of eigenfunction common to these three observable. These eigenfunctions must

then satisfy the system of differential equations

$$
\begin{align}
H\psi(\mathbf{r}) &= E_n\psi(\mathbf{r}) \tag{3.3}\\
\mathbf{L}^2\psi(\mathbf{r}) &= l(l+1)\hbar^2\psi(\mathbf{r}) \tag{3.4}\\
L_z\psi(\mathbf{r}) &= m\hbar\psi(\mathbf{r}), \tag{3.5}
\end{align}
$$

The eigenvalues of the three operators are determined with the three quantum numbers n, l and m.

- n is the *principal quantum number* and can take any non-negative integer value. It determines the major energy state E_n of the atom by the relation

$$
E_n = -\frac{E_I}{n^2}, \tag{3.6}
$$

  with E_I depending on the properties of the atom ($E_I = 13.6$ eV for the hydrogen atom).

- l is the *orbital quantum number* which describes the magnitude of the orbital angular momentum of the electron. It can take any integer value between 0 and $n-1$.

- m is the *magnetic quantum number* and describes the direction of orbital angular momentum. It is confined by the orbital quantum number l and may assume integer values ranging from $-l$ to $+l$.

- *Spin s* is the intrinsic angular momentum of the electron and may assume values $-\frac{1}{2}$ or $\frac{1}{2}$.

The resolution of this system provides eigenfunctions of the form

$$
\psi(\mathbf{r}) = R_{nl}(r)Y_{lm}(\theta, \phi). \tag{3.7}
$$

The radial wavefunction depends only on n and l, while the spherical harmonics depends on l and m.

The *Pauli exclusion principle* states that two electron (which are fermions) cannot be in the same state and then cannot have the same set of four quantum numbers (n, m, l and s).

3.1.2 Selection rules for transitions

The transition involving a single electron are submitted to some selection rules:

- The change in orbital quantum number for an allowed transition must be -1 or $+1$.

- The change in magnetic quantum number must be -1, 0 or $+1$.

- The change in spin must be 0.

- The change in $j = |l+s|$ must be 0, -1 or $+1$ but a transition from $j = 0$ to $j = 0$ is not allowed.

3.1.3 Fine structure

The fine structure is due to small interactions that give small shifts and splittings of the energy levels. They may be analyzed by means of perturbation theory. The fine structure of hydrogen is actually two separate corrections to the Bohr energies: one due to the relativistic motion of the electron, and the other due to spin-orbit coupling.

Relativistic shifts

The degeneracy for levels of different l but equal n is lifted by relativistic effects. The kinetic energy of a particle of mass m is given by

$$T = (c^2 \mathbf{p}^2 + m^2 c^4)^{\frac{1}{2}} - mc^2 = \frac{\mathbf{p}^2}{2m} - \frac{1}{2mc^2} \left(\frac{\mathbf{p}^2}{2m}\right)^2 + \dots \qquad (3.8)$$

Then we can write the hamiltonian $H = H_0 + H'$, where H_0 is the non-relativistic hamiltonian. The perturbation H' is given by

$$H' = -\frac{1}{2mc^2} \left(\frac{\mathbf{p}^2}{2m}\right)^2 = -\frac{1}{2mc^2} (H_0 - V(r))^2 \qquad (3.9)$$

We calculate the relativistic correction to the energy by first-order perturbation theory which consists of assuming that the eigenfunction of the relativistic hamiltonian are identical to the eigenfunctions ψ_n of the non-relativistic hamiltonian.

Spin-orbit interaction

Orbiting electron produces a magnetic field to which the spin magnetic moment couples. This coupling is closely related to the Zeeman coupling and is know as the spin-orbit interaction. This interaction can be estimated by considering the velocity-induced magnetic field experienced by an electron moving through the electric field of the nucleus. The spin-orbit term of the hamiltonian can be written as

$$H_{SO} = \xi(r) \mathbf{L}.\mathbf{S} \qquad (3.10)$$

By adding the terms due to the relativistic shift and to the spin-orbit interaction, one can finally obtain the the total energy shift of the fine structure

$$\Delta E_{\text{Total}} = \Delta E_{\text{rel}} + \Delta E_{\text{LS}} = -E_n \frac{\alpha^2 Z^2}{n^2} \left(\frac{3}{4} - \frac{n}{j + 1/2}\right), \qquad (3.11)$$

where $\alpha = e^2/4\pi\epsilon_0 \hbar c$ is the *fine structure constant*.

3.1.4 Hyper-fine structure

According to classical thinking, the electron moving around the nucleus has a magnetic dipole moment, because it is charged. The interaction of this magnetic
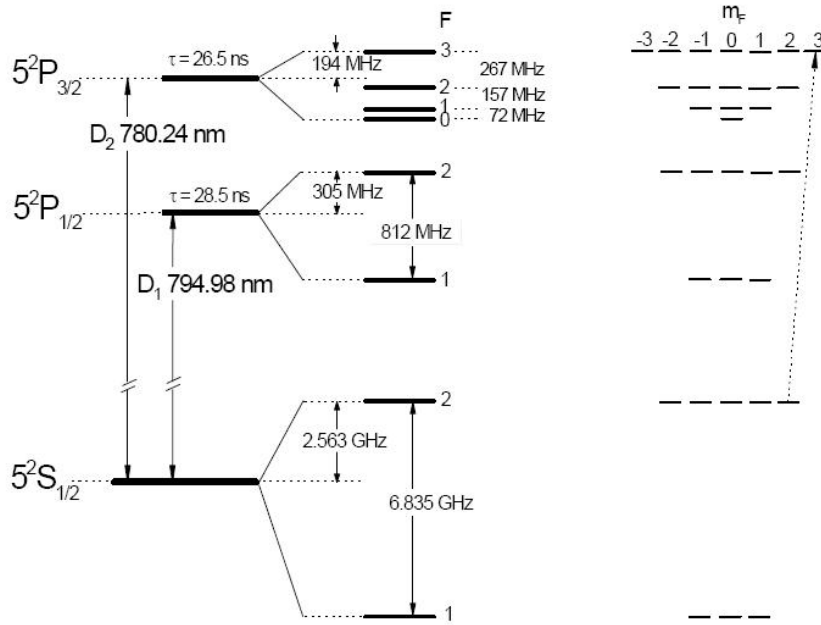
Figure 3.1: Energy levels scheme of the two lowest excited levels of ^{87}Rb

dipole moment with the magnetic moment of the nucleus leads to hyperfine splitting.

The nuclear spin $\mathbf{I}$ and the total electron angular momenta $\mathbf{J} = \mathbf{L} + \mathbf{S}$ get coupled giving rise to the total angular momentum $\mathbf{F} = \mathbf{J} + \mathbf{I}$. According to the *Landé interval rule*, the energy level is split into $(J + I) - |J - I| + 1$ energy levels. These levels are represented by the quantum number F which can take the values $|J - I|$, $|J - I| + 1$,...,$J + I$.

3.1.5   The example of ^{87}Rb

The Figure 3.1 shows the energy levels scheme of the two lowest excited levels of ^{87}Rb. In the spectroscopic notation, $5p_{3/2}$ means $n = 5$, $l = 1$ (s,p,d,f...) and $j = |l+s| = 3/2$ ($s = +1/2$). The energy difference between the levels $5p_{1/2}$ and $5p_{3/2}$ is due to the fine structure (spin-orbit interaction + relativistic shifts). The hyperfine-structure is represented by the F levels, while the sublevels are described by the quantum number m_F which can take any integer value between $-F$ and $+F$. In presence of magnetic field, those sublevels are shifted. The Zeeman effect is described for an hydrogen atom in a uniform magnetic field in Appendix B.2. However in the case of Rubidium, l and m must be replaced by F and m_F. The Zeeman sublevels also involve optical transitions depending on

18

the polarization of the incident field (see Section 3.2.2).

3.2 Interaction of an atom with an electro-magnetic wave

3.2.1 Electric dipole transition

The electric dipole moment of a single-electron atom is given by [15]

$$\mathbf{d} = -e\mathbf{r}. \tag{3.12}$$

Let be $\hat{\epsilon}$ the polarization of the incident monochromatic electric field. We can then define the electric dipole operator $H_{ED} = \hat{\epsilon} \cdot \mathbf{d}$. The matrix element $< g|H_{ED}|e >$ of this operator between the ground state $|g >$ and the excited state $|e >$ describes the interaction between the dipole induced in the atom and the electromagnetic field which is resonant if the frequency of the latter corresponds to the energy difference between the initial and final states of a transition.

$$
\begin{aligned}
< g|H_{ED}|e > &= \hat{\epsilon} \cdot < e|\mathbf{d}|g > & (3.13) \\
&= \hat{\epsilon} \cdot \mathbf{D}_{eg} & (3.14) \\
&= (\hat{\epsilon} \cdot \hat{r}_{eg})D_{eg}, & (3.15)
\end{aligned}
$$

where $\mathbf{D}_{eg} = \hat{r}_{eg}D_{eg}$ is known as the transition dipole moment. Its direction defines the direction of transition polarization, and its square determines the strength of the transition.

3.2.2 Polarization aspects

According to the fact that the atoms are quantized along the Oz axis, we define an orthonormal basis $\{\hat{u}_q; q \in \{-1, 0, 1\}\}$ for the polarization of the incident electric field

$$
\begin{aligned}
\hat{u}_{+1} &= -\frac{1}{\sqrt{2}}(\hat{x} + i\hat{y}) & (3.16) \\
\hat{u}_0 &= \hat{z} & (3.17) \\
\hat{u}_{-1} &= \frac{1}{\sqrt{2}}(\hat{x} - i\hat{y}) & (3.18)
\end{aligned}
$$

$\hat{u}_{+1}$ and $\hat{u}_{-1}$ are two orthogonal circular polarizations in the xOy plane.

σ^+, π and σ^- transitions

We can now decompose the polarization of the electric field $\hat{\epsilon}$ in the basis $\{\hat{u}_q; q \in \{-1, 0, 1\}\}$

$$\hat{\epsilon} = \sum_q \epsilon_q \hat{u}_q \tag{3.19}$$

19

For hydrogen-like atoms, we can write the ground state $|nlm>$ and the excited state $|n'l'm'>$, then we obtain

$$\hat{\epsilon} \cdot \mathbf{D}_{eg} = -e \sum_q \epsilon_q < n'm'l'|\hat{u}_q \cdot \mathbf{r}|nml > \tag{3.20}$$

By using spherical harmonics, one can obtain that the term $< n'm'l'|\hat{u}_q \cdot \mathbf{r}|nml >$ has a non-zero value only if $m' - m = q$. The matrix element can then be simplified

$$\hat{\epsilon} \cdot \mathbf{D}_{eg} = -e \, \epsilon_{m'-m} < n'm'l'|\hat{u}_{m'-m} \cdot \mathbf{r}|nml > . \tag{3.21}$$

Only the projection of the electric field on the $\hat{u}_{m'-m}$ polarization interacts with the transition.

We can consider for example the transition between the levels $|100>$ and $|21m>$ of the hydrogen atom, with an electric field polarized along $\hat{u}_{+1}$ (it is called a $\sigma+$ polarization). If the frequency of the electric field is sufficiently close to the frequency of the transition [1], an atom in the ground state $|100>$ can absorb a $\sigma+$ polarized photon and then be lifted in the $|211>$ state. Inversely, a photon spontaneously emitted from the state $|211>$ to the state $|100>$ will be $\sigma+$ polarized.

We define three types of transition which depend on the value of $\Delta m = m' - m$

- $\Delta m = +1$: σ_+ transition

- $\Delta m = 0$: π transition

- $\Delta m = -1$: σ_- transition.

We can note that in the case of Rubidium, these transitions involve the Zeeman sublevels (m_F).

3.2.3   Optical Bloch Equations

We consider in this section a single atom at rest with only two discrete non-degenerate states, the ground state g and the first excited state e located at a distance $\hbar\omega_0$ above g and having a natural width γ [2]. We consider the case where the atom interact with a monochromatic field whose frequency ω is very close to the atomic eigenfrequency ω_0.

The optical Bloch equation link the component of the density matrix which is briefly described in Appendix B.4.1:

$$\begin{cases} \dot{\rho}_{ee} = -\frac{i\Omega}{2}(\rho_{ge} - \rho_{eg}) - 2\gamma\rho_{ee} = -\dot{\rho}_{gg} \\ \dot{\rho}_{eg} = \frac{i\Omega}{2}(\rho_{gg} - \rho_{ee}) + (i\delta - \gamma)\rho_{eg} = -\dot{\rho}_{ge}^*, \end{cases} \tag{3.22}$$

---

[1] We consider that the three levels $|21m>$ have the same energy. This is not true in presence of a magnetic field (See Appendix B.2)

[2] The natural width γ is related to the life time τ by the relation $\gamma = 2/\tau$

where $\delta = \omega - \omega_0$ is the detuning from the center of the resonance and

$$\Omega = \frac{E_0(\hat{\epsilon} \cdot \mathbf{D}_{eg})}{\hbar} \qquad (3.23)$$

is the Rabi frequency of the $g \leftrightarrow e$ coherence. The Rabi frequency does not only depend on the amplitude of the incident electric field but also on its polarization. One can obtain the steady-state solution of the optical Bloch equations by setting the time-derivatives to zero

$$\rho_{ee} = \frac{\Omega^2}{4} \frac{1}{\delta^2 + \gamma^2 + \frac{1}{2}\Omega^2} = 1 - \rho_{gg} \qquad (3.24)$$

$$\rho_{ge} = -\frac{\Omega}{2} \frac{\delta - i\gamma}{\delta^2 + \gamma^2 + \frac{1}{2}\Omega^2} = \rho_{eg}^*. \qquad (3.25)$$

We define the two-level saturation parameter s_0 as

$$s_0 = \frac{\Omega^2}{\gamma^2}. \qquad (3.26)$$

Equation 3.23 shows that Ω^2 is proportional to the classical coherent incident beam intensity $\bar{I}$. We can then define the saturation intensity $\bar{I}_s$ by the relation

$$s_0 = \frac{\bar{I}}{\bar{I}_s}. \qquad (3.27)$$

In the low intensity regime ($s_0 \ll 1$), the fractional excited state occupation is a Lorentzian function of the "detuning" δ/γ

$$\rho_{ee} \simeq \frac{s_0/2}{1 + (\delta/\gamma)^2}. \qquad (3.28)$$

We have moreover on resonance $\rho_{ee} \simeq s_0/2$.

When the saturation parameter increases, the width of the Lorentzian increases while the excited state occupation tends to its maximum value $\rho_{ee}^{\mathrm{max}} = 1/2$.

In the case of unit-saturation ($s_0 = 1$), we have on resonance $\rho_{ee} = 1/4$. The increase of the intensity beyond the saturation intensity broadens the Lorentzian but doesn't have much effect on the excited state occupation.

The induced electric-dipole moment of the atom is given by [14]

$$d(t) = -\left(\rho_{eg}(\hat{\epsilon} \cdot \mathbf{D}_{eg})e^{-i\omega t} + \rho_{ge}(\hat{\epsilon} \cdot \mathbf{D}_{ge})e^{i\omega t}\right) \qquad (3.29)$$

$$= -e\frac{\Omega}{2}(\hat{\epsilon} \cdot \mathbf{D}_{eg})\left(\frac{\delta - i\gamma}{\delta^2 + \gamma^2 + \frac{1}{2}\Omega^2}e^{-i\omega t} + c.c.\right) \qquad (3.30)$$

3.2.4 Refractive index and extinction coefficient of dilute gases

Classical electric susceptibility

The electric susceptibility χ of a medium is a measure of how easily it polarizes in response to an electric field. It is defined as the constant of proportionality (which may be a tensor) relating an electric field $\mathbf{E}$ to the induced dielectric polarization density $\mathbf{P}$ such that

$$\mathbf{P} = \epsilon_0 \chi \mathbf{E} \tag{3.31}$$

The electric displacement $\mathbf{D}$ is related to the polarization density $\mathbf{P}$ by

$$\mathbf{D} = \epsilon_0 \mathbf{E} + \mathbf{P} = \epsilon_0 (1 + \chi) \mathbf{E} = \epsilon_0 \epsilon_r \mathbf{E}, \tag{3.32}$$

where ϵ_r is the relative permittivity of the medium.

However, a medium cannot polarize instantaneously in response to an applied field then we rewrite Equation 3.31 as a convolution

$$\mathbf{P}(t) = \epsilon_0 \int_{-\infty}^{t} \chi(t - t') \mathbf{E}(t') \, dt'. \tag{3.33}$$

In the Fourier's space, this relation becomes

$$\mathbf{P}(\omega) = \epsilon_0 \chi(\omega) \mathbf{E}(\omega). \tag{3.34}$$

The complex refractive index $\eta(\omega)$ is related to the linear susceptibility $\chi(\omega)$ through

$$\eta^2(\omega) = 1 + \chi(\omega) \tag{3.35}$$

The real part $\eta'(\omega)$ of $\eta(\omega)$ is the *refractive index* while its imaginary part $\eta''(\omega)$ is the *extinction coefficient*.

Electric susceptibility of dilute gases

Let $\mathbf{d}(t)$ be the averaged dipole moment per atom at time t (see Section 3.2.1). The macroscopic polarization of the gas is then simply [14]

$$\mathbf{P}(t) = \frac{N}{V} \mathbf{d}(t), \tag{3.36}$$

where N is the number of atoms and V the volume of the gas sample. Using the relations 3.29 and 3.34, one can obtain the expression for the electric susceptibility

$$\chi(\omega) = \frac{-eN(\hat{\epsilon} \cdot \mathbf{D}_{eg})^2}{2V\epsilon_0 \hbar} \left(\frac{\delta - i\gamma}{\delta^2 + \gamma^2 + \frac{1}{2}\Omega^2} \right). \tag{3.37}$$

In the case of dilute gases, the electric susceptibility is sufficiently small to write

$$\eta(\delta) \quad \simeq \quad 1 + \frac{1}{2}\chi(\omega) \tag{3.38}$$

$$= \quad \eta'(\delta) + \eta''(\delta), \tag{3.39}$$

where

$$\eta'(\delta) = 1 + \frac{-eN(\hat{\epsilon} \cdot \mathbf{D}_{eg})^2}{4V\epsilon_0\hbar} \left(\frac{\delta}{\delta^2 + \gamma^2 + \frac{1}{2}\Omega^2} \right) \tag{3.40}$$

is the refractive index of the gas and

$$\eta''(\delta) = \frac{-e\gamma N(\hat{\epsilon} \cdot \mathbf{D}_{eg})^2}{4V\epsilon_0\hbar} \left(\frac{1}{\delta^2 + \gamma^2 + \frac{1}{2}\Omega^2} \right) \tag{3.41}$$

is the extinction coefficient of the gas. The absorption of the gas is then a Lorentzian function of the detuning while the phase shift is proportionnal to the derivative of a Lorentzian.

3.3 Absorption spectrum

A medium's absorption spectrum shows the fraction of incident electromagnetic radiation absorbed by the medium over a range of frequencies. If the frequency of the incident light coïncide with the frequency of a certain transition, the atoms of the medium can absorb a photon while a valence electron make transition between the two concerned energy levels. If the frequency ω of the incident radiation does not exactly equals the frequency of the transition, there is still a probability that an atom absorbs a photon of energy $\hbar\omega$. We show in Section 3.2.3 that this probability is a Lorentzian function of the detuning $\delta = \omega - \omega_0$. This results in a broadening of the absorption line. From Equation 3.24, we see that the FHWM [3] of the Lorentzian absorption profile is

$$\Gamma_{\text{FWHM}} = \sqrt{\gamma^2 + \frac{1}{2}\Omega^2} \tag{3.42}$$

$$= \gamma\sqrt{1 + \frac{1}{2}s_0} \tag{3.43}$$

The line-width of the absorption line is then limited by the natural width γ of the excited level. In order to perform a good S/N ratio, we would like to use strong intensities which will unfortunately broaden the absorption line. We then have to reach a compromise between the S/N ratio and the broadening. We can consider that this compromise is reached around the unit saturation ($s_0 \approx 1$).

3.3.1 Doppler broadening

Let's consider a planar monochromatic wave of frequency ω propagating through a gas sample along the Oz axis. The frequency of the light experienced by an atom of the sample is given by the relation

$$\omega(v_z) = \omega \cdot (1 + \frac{v_z}{c}) \tag{3.44}$$

_____

[3]Full Width at Half-Maximum

where v_z is the projection of the velocity of the atom along the Oz axis. Therefore, atoms with different velocities will absorb preferentially photons of different frequencies. This phenomenon results in a broadening of the spectra.

In a gas sample, the probability distribution $P(v_z)$ of the velocity v_z is given by the Maxwell's distribution:

$$P(v_z) = \left(\frac{m}{2\pi k_B T}\right)^{\frac{3}{2}} e^{-\frac{mv_z^2}{k_B T}} \tag{3.45}$$

Using Equations (3.44) and (3.45), one can obtain the width (FWHM)$\Delta\omega_{\text{Doppler}}$ of the doppler-broadened gaussian absorption spectrum

$$\Delta\omega_{\text{Doppler}} = 2\omega_0 \sqrt{2\ln 2 \frac{k_B T}{mc^2}} \tag{3.46}$$

where we have considered that the doppler-free spectrum is a dirac centered on ω_0. A simple calculation for ^{87}Rb at room temperature shows that the Doppler broadening is much larger than the natural linewidth of the excited state.

$$\Delta f = 505\,\text{MHz} \tag{3.47}$$

We need to lock our laser with an accuracy of 1 MHz, we then need to know the frequency of the laser beyond the Doppler limit. We then use locking methods which are freed of the Doppler broadening. Doppler-free spectroscopy is described in Chapter 4.

Chapter 4

Locking a laser on a optical line

4.1 General scheme

Locking a laser means stabilizing the frequency of the laser using a reference frequency. The difference between the frequency of the laser and the reference frequency gives an error signal which can be used as a feedback to lock the laser. The reference frequency can be defined by a Fabry-Pérot etalon, this is the purpose of the Pound-Drever-Hall method [3]. This method provides the possibility of tuning the frequency of the laser by tuning the resonance frequency of the etalon.

We only need to be able to lock a laser on optical transition of ^{87}Rb in order to drive them in a magneto-optical trap to perform Bose-Einstein condensation. We will use a gas cell containing only the ^{87}Rb isotope. By observing the changes in the properties of the light passing through the cell, we will be able to compare the frequency of the laser with the frequency of the transition.

We explore in this section the methods which can be used to lock a laser on a optical transition of the ^{87}Rb using a gas cell.

4.2 Saturation spectroscopy

Saturation spectroscopy [2] constitutes the basis of Doppler-free spectroscopy. Other classical methods like polarization spectroscopy actually derive from saturation spectroscopy.

4.2.1 Principle

Saturation spectroscopy is based on the interaction of a pump beam and a counter-propagating probe beam at the same frequency crossing in a cell. Let be ω_0 the frequency of the transition and ω the frequency of the pump beam

(and then also of the probe beam), close to ω_0. Because of the Doppler effect, the pump beam is absorbed by the atoms which belong to a certain velocity class $\mathcal{V}(\omega)$ defined by

$$\mathcal{V}_{\text{pump}}(\omega) = \{v_z, \ |\omega(1 + \frac{v_z}{c}) - \omega_0| \leqslant \frac{\Gamma}{2}\}, \tag{4.1}$$

where Γ is the linewidth (FWHM) of the absorption profile of the transition (see Section 3.3). For small intensities of the pump beam, we have $\Gamma \simeq \gamma$, where γ is the natural linewidth of the transition. The counter-propagating probe beam is supposed to have an intensity much smaller than the intensity of the pump beam which is usually of the order of the saturation intensity. The probe beam is absorbed by the atoms which belong to the velocity class

$$\mathcal{V}_{\text{probe}}(\omega) = \{v_z, \ |\omega(1 - \frac{v_z}{c}) - \omega_0| \leqslant \frac{\Gamma}{2}\}, \tag{4.2}$$

The velocity class of atom interacting simultaneously with the pump and the probe beam $\mathcal{V}(\omega)$ is

$$\mathcal{V}(\omega) = \mathcal{V}_{\text{pump}}(\omega) \cap \mathcal{V}_{\text{probe}}(\omega). \tag{4.3}$$

We then $\mathcal{V}(\omega) \neq \phi$ differs from the empty set only if $|\omega - \omega_0| \leq \frac{\Gamma}{2}$. In this case we have

$$\mathcal{V}(\omega) = \{v_z, \ |\frac{v_z}{c}| \leqslant |\frac{\Gamma}{2} - |\omega - \omega_0||\}. \tag{4.4}$$

Then when $|\omega - \omega_0| \leq \frac{\Gamma}{2}$, the atoms interacting with the probe beam have been already partially pumped into the upper state of the transition by the pump beam. The probe beam is then less absorbed. The dip created in the absorption spectra is called *Lamb dip*. The Lamb dip is centered on ω_0 and has a width (FWHM) of $\frac{\Gamma}{2}$, it is then a Doppler-signal. It is an absorptive signal i.e. an even function of the detuning $\delta = \omega - \omega_0$. One cannot then directly use it as an error signal to lock the laser because it does not provide the sign of δ. In order to lock the laser, one has to take the derivative of this signal which is an odd function of δ (dispersive signal). This signal can be directly used as an error signal because it is proportional to δ when δ is sufficiently small. The lines obtained with interaction of atoms with zero longitudinal velocities are called *pure lines* (PL)

Crossover lines

Crossover lines (CO) are produced when the pump and the probe beam run different transitions of frequencies respectively ω_1 and ω_2. When the frequency ω of the probe and the pump beam is exactly midway between ω_1 and ω_2, the probe and the pump beam are resonant simultaneously with the same velocity class of atoms. The atoms belonging to this velocity class have unlike for the case of pure lines a finite value.

4.2.2 FM spectroscopy

FM spectroscopy [4] is a method used to obtain a dispersive signal from an absorptive signal. The probe beam is modulated in phase at radio-frequencies. A photodiode placed after the cell give the absorptive signal. This signal is then mixed with the modulation signal. The DC part of the mixer's output is proportional to the derivative of the absorptive signal and then can be directly used to lock the laser. However, FM spectroscopy is actually more complex and one can read the articles [3] and [4] for further comprehension.

4.3 Polarization spectroscopy

4.3.1 Principle

As in saturation spectroscopy, polarization spectroscopy is a method in which the effect of a pump beam on the transmission of a counter-propagating beam is exploited to provide Doppler-free signals. The pump beam is usually σ^+ polarized and the probe beam is linearly polarized.

$$\mathbf{E}_{probe} = E_0(\cos(\theta)\mathbf{x} + \sin(\theta)\mathbf{y}). \tag{4.5}$$

The pump beam induces changes in absorption coefficient ($\Delta\alpha_+$ and $\Delta\alpha_-$)and refractive index (Δn_+ and Δn_-), $+$ and $-$ corresponding to the two orthogonal circular polarizations σ^+ and σ^- (See Appendix B.1). A difference $\Delta\alpha_+ - \Delta\alpha_-$ describes a circular dichroism which will make the probe beam linearly polarized, and a difference $\Delta n_+ - \Delta n_-$ describe a gyrotropic birefringence which will rotate the axis of polarization.

4.3.2 Dichroism: absorptive signal

The absorption coefficients $\Delta\alpha_+$ and $\Delta\alpha_-$have been computed by C. Wieman and T.W. Hänsch [1]:

$$\Delta\alpha_+ = \Delta\alpha_-/d = -\frac{\alpha_0}{2}\frac{I}{I_{sat}}\frac{1}{1+x^2}, \tag{4.6}$$

where α_0 is the unsaturated background absorption, I is the intensity of the polarizing beam, I_{sat} is the saturation parameter, and $x = (\omega - \omega_0)/\gamma$ describes the laser detuning from resonance. The parameter $d = \Delta\alpha_-/\Delta\alpha_+$ only depends on F, F' and the decay rates of both the levels. We can then obtain

$$\Delta\alpha = \frac{\Delta\alpha_+ - \Delta\alpha_-}{2} = \frac{-\alpha_0(1-d)}{4}\frac{I}{I_{sat}}\frac{1}{1+x^2}. \tag{4.7}$$

Hence, the dichroism $\Delta\alpha$ is a Lorentzian function of the detuning and cannot be used directly to lock a laser. However, one can obtain a derivative signal from the dichroism using FM modulation techniques.

4.3.3 Birefringence: dispersive signal

The gyrotropic birefringence has the advantage to provide immediately a dispersive signal. According to the Kramers-Krönig relation which connects the real and the imaginary part of any analytic function, we can write

$$\Delta n_{\pm} = \frac{-c}{2\omega}\Delta\alpha_{\pm}x, \qquad (4.8)$$

then

$$\Delta n = \frac{\Delta n_+ - \Delta n_-}{2} = \frac{c}{2\omega}\frac{\alpha_0(1-d)}{4}\frac{I}{I_{sat}}\frac{x}{1+x^2}. \qquad (4.9)$$

Near resonance (i.e. $x \ll 1$), Δn is proportional to the detuning x. Hence, any signal proportional to Δn can be used directly to lock a laser. In Appendix B.1, we show that the gyrotropic birefringence rotates any incoming linear polarization with an angle proportional to Δn.

To detect the light-induced birefringence, the usual scheme is to place the cell between two crossed polarizers so as to detect the rotation of the probe beam [1]. This scheme is simple but the residual background light cannot be eliminated and then degrades the S/N ratio. Y. Yoshikawa & al. [5] explored a slightly modified scheme using balanced detection between two orthogonal polarization components of the probe beam. This results in a background free spectra with an improved S/N ratio. We use this method for our locking experiment. It is called DLIB for Doppler-free light-induced birefringence. This is both a modulation-free and a magnetic field-free method. However, the Zeeman shift caused by the ambient magnetic field modifies the error signal as shown in Figures 4.1 and 4.2. Strong magnetic fields alter the shape of the DLIB spectrum (the dispersive signals becomes absorptive); while weak fields [1] leave the global shape of the DLIB spectrum unchanged but shift the zero crossing point(and then shift the locking frequency). Furthermore, inhomogeneous magnetic field broadens the dispersive signal and then must be avoided as far it is possible. The cell must then be shielded from magnetic field, it is described in section 4.5.

4.4 Experimental setup of DLIB spectroscopy

Figure 4.3 shows the schematic diagram of the experimental setup. The angle between the probe beam and the pump beam is emphasized in the figure [2]. The first half wave-plate is used to control the intensity of the probe and the pump beam. The intensity of the pump beam equals roughly the saturation intensity (1.6 mW/cm^2), while the probe beam is 10 times weaker.

We encountered some difficulties while realizing the setup:

- The feedback into the DFB laser induces mode-hops which can stop the possibility to scan the whole spectrum of Rubidium. This feedback is

---

[1] Weak field means here that the Zeeman shift is small compared to the natural linewidth of the transition.

[2] The angle is actually about 3 degrees.

28
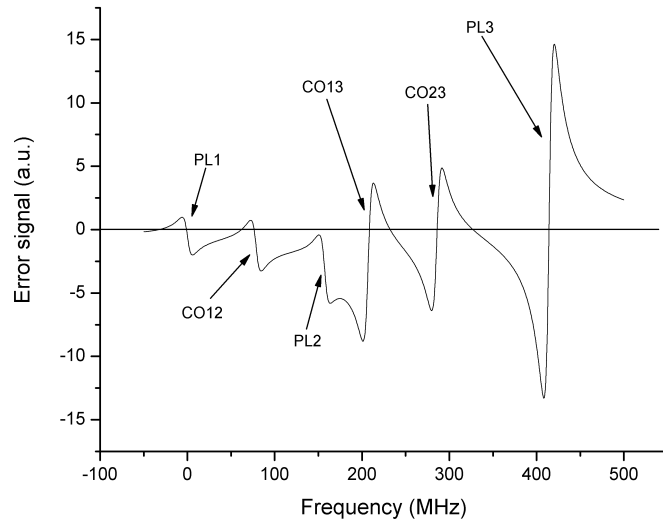
Figure 4.1: Theoretical plot of the DLIB error signal vs. the frequency of the laser with zero magnetic field

$PL2$ means the transition from $5S_{\frac{1}{2}} F = 2$ to $5P_{\frac{1}{2}} F' = 2$ and $CO13$ means the cross-over line between the $PL1$ and $PL3$ line
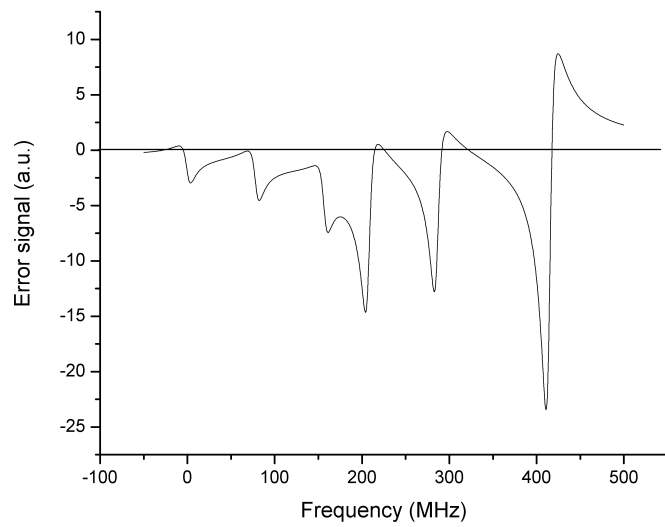
Figure 4.2: Theoretical plot of the DLIB error signal vs. the frequency of the laser with presence of magnetic field (Zeeman shift of 3 MHz)
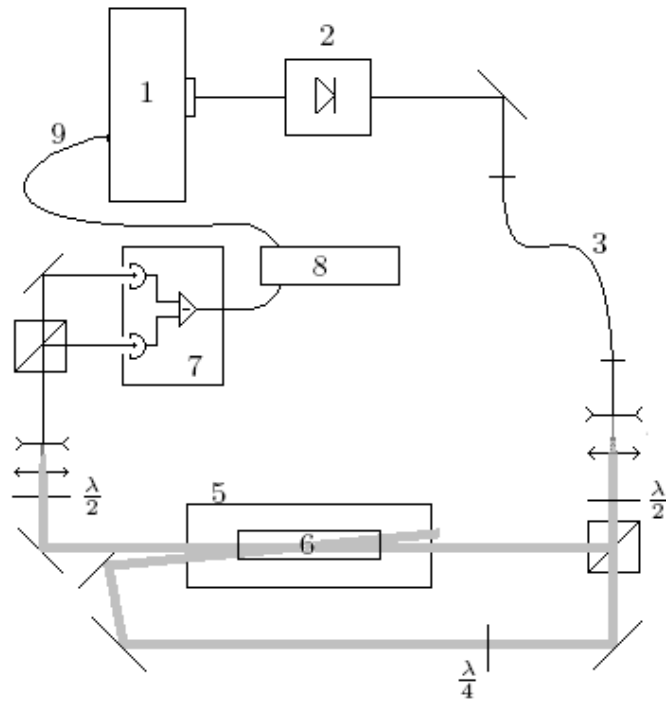
Figure 4.3: Scheme of the setup of DLIB spectroscopy
1. DFB Laser, 2. 60 dB isolator, 3. Monomode fiber, 4. Polarizing beam splitter cube, 5. Magnetic shield, 6. Rubidium gas cell, 7. Balancing system, 8. Locking box, 9. Current control
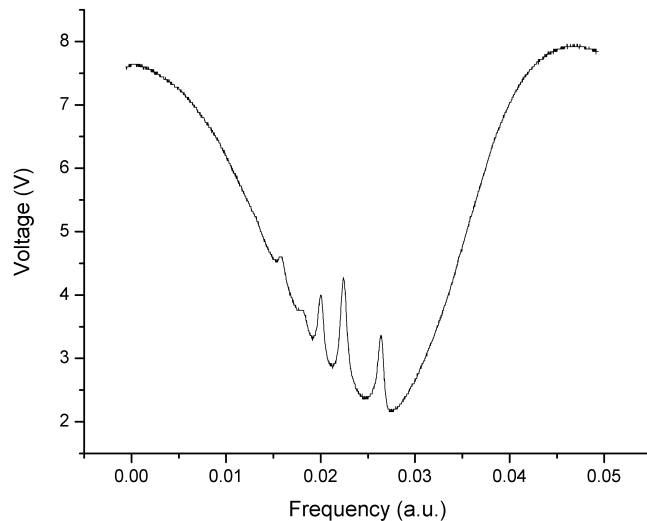
Figure 4.4: Saturation spectroscopy absorption spectrum obtained by blocking one of the two photodiodes

especially important with the presence of a Fabry-Pérot etalon in the setup but a 60dB-isolator is sufficient to prevent feedback.

- The optical table produces a strongly inhomogeneous magnetic field, we had to lift the cell with 15 cm.

- The wave-plates and the beam-splitter cube must be checked carefully.

4.4.1 Experimental results

For the transition from from $5S_{\frac{1}{2}}F = 2$ to $5P_{\frac{1}{2}}F' = 3$ ($PL3$ in Figure 4.1), we obtain a locking signal with an amplitude of 2 V_{PP} (see Figure 4.5)while the background noise is about 20 mV. Assuming that for the pump beam is at the saturation intensity ($s = 1$) the linewidth of the locking signal is $2(1 + s)^{1/2}\Gamma = 15.6$ MHz, the zero-crossing point of the locking signal is then defined with an accuracy of about 200 kHz. However, this does not prevent long-term drifts of the frequency of the zero-crossing point. We can observe that the experimental spectrum differs from the calculated spectrum. The $CO13$ and $CO23$ lines does not cross the zero level as expected in the calculation. This result can be explained by the presence of a residual magnetic field. The magnetic field can generate a background which has a dispersive shape. This
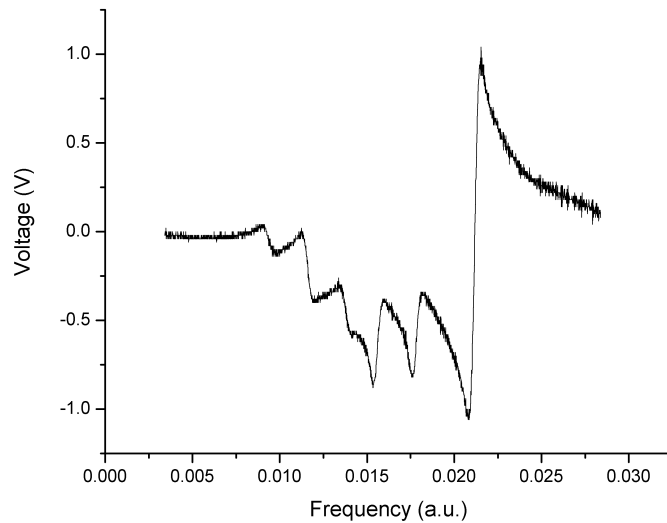
32

Figure 4.5: Experimental DLIB spectrum of ^{87}Rb $D2$ line

background is obtained by the substraction of two Doppler-broadened profiles each Zeeman-shifted in opposite directions. To conclude, this method provides a locking signal with a huge signal to noise ratio but however this method has the disadvantage to be very sensitive to the magnetic field. Sometimes it is more easy to produce a magnetic field than to shield against it. Those shielding aspects are described in the next section.

4.5   Magnetic aspects

4.5.1   Zeeman effect

The Zeeman effect is the splitting of a spectral line into several components in the presence of a static magnetic field. We show in Appendix B.2 that the Zeeman effect changes not only the frequency, but also the polarization of the atomic lines. Those properties can be used for spectroscopy, but for the same reasons it can be necessary to realize a magnetic shielding to prevent from these effects.

4.5.2   Utilization of the Zeeman effect in spectroscopy

We can cite a method [6] which makes use of the Zeeman effect to get a dispersive signal. It is saturation spectroscopy, but the cell is immersed in a magnetic
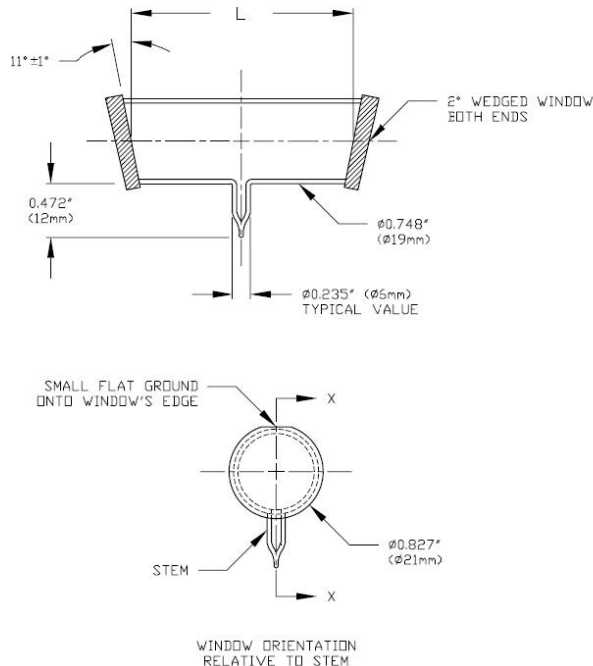
Figure 4.6: Scheme of the *Thorlabs* gas reference cell

field which induces Zeeman shifts. The σ^+ and σ^- components of the linearly polarized probe beam are both generating a saturated absorption profile, each Zeeman-shifted by the same amount but in opposite directions. The dispersive signal is obtained by separately detecting the two components and subtracting their signals from each other.

4.5.3   Magnetic shielding

In order to lock the Laser on a specific transition of Rubidium, we use a quartz reference cell manufactured by *Thorlabs*. This cell only contains the ^{87}Rb isotope at the pressure of 4 Torr. A scheme of the cell is given in Figure 4.6. The windows are designed with a 2 degrees wedge to eliminate the etalon effects of parallel surfaced windows. The wedged windows are also angled to compensate beam offset due to the index of the quartz material.

In order to prevent from magnetic perturbation such as Zeeman effect (See Section 4.5.1)), we must protect the cell with a magnetic shield. We cover the cell with two concentric tubes as shown in Figure 4.7. These tubes are covered of mu-metal, a nickel-iron alloy (75% nickel, 15% iron, plus copper and molybdenum) that has a very high magnetic permeability ($\mu = 4000$). The
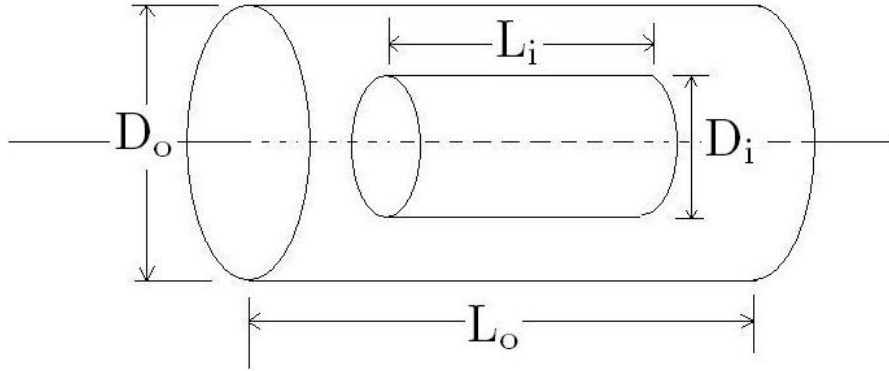
Figure 4.7: Scheme of the shield. $L_o = 200$mm, $L_i = 120$mm, $D_o = 50$mm and $D_i = 25$mm

ambient magnetic field induces at the microscopic scale magnetic dipoles in the mu-metal which tends to align with the ambient magnetic field in order to minimize their potential energy. At the macroscopic scale, the magnetic field induced by these dipoles counterbalance the ambient magnetic field which produces the shielding.

The shielding factor S [16] is defined as the ratio between the external field H_e and the internal field H_i:

$$S = \frac{H_e}{H_i}. \tag{4.10}$$

The magnetic field in the optical table is about a few Gauss, we need to reduce the magnetic field in the cell to less than 10 mGauss. We covered each tube with 5 layers of mu-metal (thickness: d = 0.2 mm). We calculated the shielding factor of the system at the windows of the cell: $S = 780$ (see Appendix B.3) which is sufficient for our experiment. So as to obtain a good shielding, we have to demagnetize the mu-metal (i.e. aligning the randomly oriented magnetic dipoles of the mu-metal with the ambient field). We realize this demagnetization by applying a decreasing alternative magnetic field [3] into each tube so as to "shake" the magnetic dipoles which can then finally align more easily with the ambient magnetic field.

---

[3] We use coils around the tubes driven by an AC current.

Practical remarks

We realized the shielding of the outer cylinder by juxtaposing two layers of mu-metal of 10 cm each. We observed that the magnetic field leaked at the boarder between the two layers. Magnetic shielding is a non-trivial science within we can expect the unexpected.

Appendix A

Fabry-Pérot resonator

A.1 Gaussian beams

The Figure A.1 gives us a scheme of the longitudinal section section of a Gaussian beam around its focus which is called the waist. For a Gaussian beam, the complex electric field amplitude at a distance r from its center, and a distance z from its waist, is given by

$$E_{00}(r, z) = E_0 \frac{w_0}{w(z)} \exp\left(\frac{-r^2}{w^2(z)}\right) \exp\left(-ikz - ik\frac{r^2}{2R(z)} + i\zeta(z)\right) \qquad \text{(A.1)}$$

Which is a paraxial solution of the Helmoltz's scalar equation. The geometry and behavior of a Gaussian beam are governed by a set of beam parameters, which are defined in the following sections.

For a Gaussian beam propagating in free space, the spot size (which is defined by the distance from the axis where the amplitude has decreased by $1/e$) $w(z)$ will be at a minimum value w_0 at one place along the beam axis, known as the "beam waist". For a beam at a distance z from the beam waist, the variation of the spot size is given by

$$w(z) = w_0 \sqrt{1 + \left(\frac{z}{Z_R}\right)^2} \qquad \text{(A.2)}$$

where the origin of the z-axis is defined to coincide with the beam waist, and where

$$z_R = \frac{\pi w_0^2}{\lambda} \qquad \text{(A.3)}$$

is called the "Rayleigh range". At a distance from the waist equal to the Rayleigh range Z_R, the width of the beam is

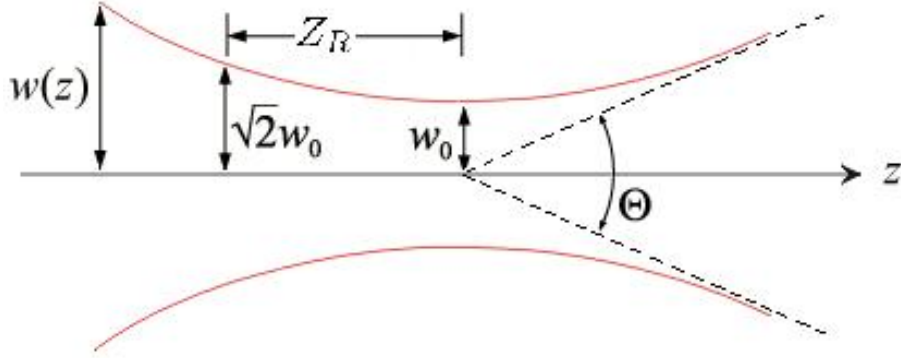$$w(\pm Z_R) = w_0 \sqrt{2}. \qquad \text{(A.4)}$$

Figure A.1: Gaussian beam parameters

The distance between these two points is called the confocal parameter of the beam:

$$b = 2Z_R = \frac{2\pi w_0^2}{\lambda} \ . \tag{A.5}$$

$R(z)$ is the radius of curvature of the wavefronts comprising the beam. Its value as a function of position is

$$R(z) = z \left[1 + \left(\frac{Z_R}{z} \right)^2 \right] \tag{A.6}$$

The parameter $w(z)$ approaches a straight line for $z \gg Z_R$. The angle between this straight line and the beam's central axis is called the divergence of the beam. It is given by

$$\theta \simeq \frac{\lambda}{\pi w_0} \qquad (\theta \text{ in radians}). \tag{A.7}$$

The total angular spread of the beam far from the waist is then given by : $\Theta = 2\theta$.

The longitudinal phase delay or Gouy phase of the beam is

$$\zeta(z) = \arctan \left(\frac{z}{Z_R} \right) \ . \tag{A.8}$$

A.2   Hermite-Gaussian transverse modes

The Hermite-Gaussian transverse modes are a sequence of orthogonal eigen-modes of the cavity. The amplitude of the TEM_{mn} Hermite-Gaussian transverse mode is

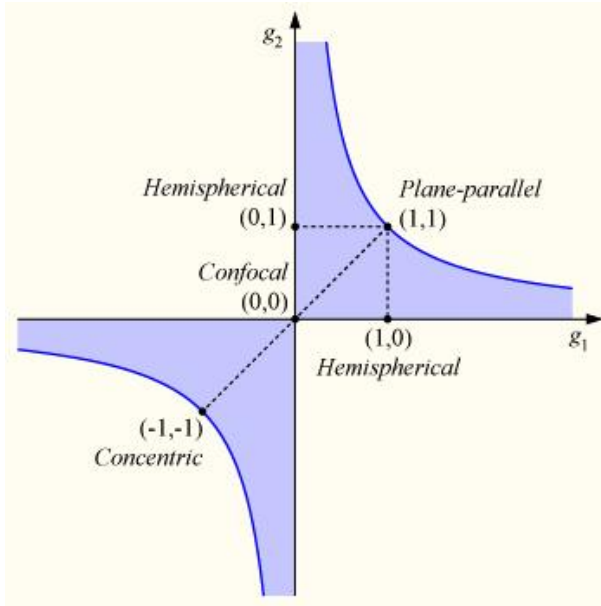$$E_{mn}(x,y,z) = E_{00}(x,y,z)\mathsf{H}_m(\sqrt{2}\frac{x}{w(z)})\mathsf{H}_n(\sqrt{2}\frac{y}{w(z)}) \exp(i(m+n)\arctan(\frac{z}{Z_R})), \tag{A.9}$$

38

Figure A.2: Stability diagram.

where H_n is the n order Hermite polynomial defined by

$$H_n(x) = (-1)^n e^{x^2} \frac{\mathrm{d}^n}{\mathrm{d}x^n}(e^{-x^2}). \tag{A.10}$$

These polynomials are orthogonal with respect to the weight function :

$$\int_{-\infty}^{\infty} H_n(x)H_m(x)\, e^{-x^2}\, \mathrm{d}x = n!\, 2^n \sqrt{\pi}\, \delta_{nm} \tag{A.11}$$

A.3 Stability of optical resonators

The study of the stability of optical resonators had been realized by Kogelnik and Li in 1966 [7]. By using ray transfer matrices, they obtained a stability condition in the form

$$0 < g_1.g_2 < 1, \tag{A.12}$$

where $g_1 = 1 - \frac{d}{R_1}$ and $g_2 = 1 - \frac{d}{R_2}$. The Figure A.3 shows the stability of the resonator versus the parameters g_1 and g_2. The stability condition shows that the confocal resonator is only marginally stable because $g_1 = g_2 = 0$. When we vary the length d of the cavity, the resonators is moving on the line "$g_2 = g_1$" on the Figure A.3. That is why if the radius of curvature of the two mirrors are strictly even, the confocal resonator cannot be unstable.
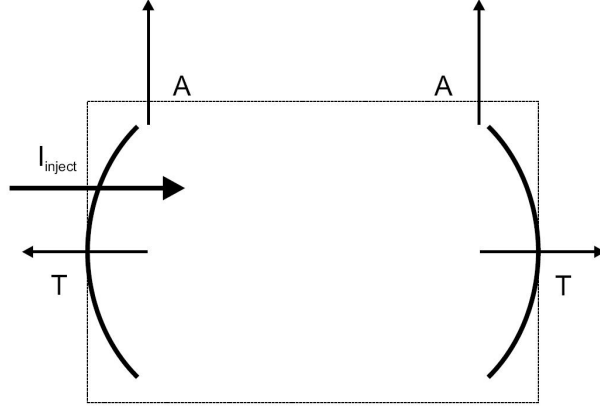
Figure A.3: Conservation of energy in an optical resonator

A.4 Effect of the losses on the efficiency of the cavity

A.4.1 Measurement of the losses of the cavity

The figure A.3 shows a schematic diagram of a Fabry-Pérot with internal losses which are represented by $\mathcal{A}$[1]. Using the conservation of energy inside the Fabry-Pérot, one can easily obtain that the maximum transmission [2] becomes [8]

$$T_{\max} = (\frac{\mathcal{T}}{\mathcal{T}+\mathcal{A}})^2, \tag{A.13}$$

while the finesse

$$\mathcal{F} = \frac{\pi\sqrt{\mathcal{R}}}{1-\mathcal{R}} \simeq \frac{\pi}{\mathcal{T}}, \tag{A.14}$$

becomes

$$\mathcal{F}' \simeq \frac{\pi}{\mathcal{T}+\mathcal{A}}. \tag{A.15}$$

We measured a transmission at the maximum of the peaks

$$T_{\max} = 0.42 \pm 5\%, \tag{A.16}$$

and a finesse

$$\mathcal{F} = 176 \pm 5\%, \tag{A.17}$$

---

[1] $\mathcal{A}$ is defined by the fraction of intensity lost at each half round-trip
[2] ratio between the intensity of the transmitted light and the intensity of the incident light at $\delta = 0$

We can obtain $\mathcal{A}$ and $\mathcal{T}$ by resolving the two simultaneous equations (A.13) and (A.15)

$$\mathcal{T} = \frac{\pi \sqrt{T_{\max}}}{\mathcal{F}} = 0.0115, \qquad (A.18)$$

while

$$\mathcal{A} = \frac{\pi (1 - \sqrt{T_{\max}})}{\mathcal{F}} = 0.0063. \qquad (A.19)$$

A.4.2   Effect of the roughness of the mirrors

The roughness of the mirrors can spoil the efficiency of the Fabry-Pérot. Because of the similarities between Helmoltz's and Schrödinger's equation, one can make this calculation using perturbation theory [9] but it is beyond the scope of this report.

For light normally incident on the surface of the mirror, the ratio Υ between the intensity of the light scattered out of the specular direction and the intensity of the incident light is given by

$$\Upsilon = (\frac{4\pi\sigma}{\lambda})^2, \qquad (A.20)$$

where σ is the RMS surface roughness of the mirror [8]. Let's assume that the scattering of the light due to the roughness of the mirrors in entirely responsible for the losses of the cavity then

$$\mathcal{A} = \Upsilon. \qquad (A.21)$$

Using (A.19) and (A.20), we obtain

$$\sigma = \frac{\lambda}{159} = 4.9 \text{ nm.} \qquad (A.22)$$

Appendix B

Spectroscopy

B.1 Polarization

B.1.1 General considerations

We consider in this section a frame $(\mathbf{x}, \mathbf{y}, \mathbf{z})$ and a monochromatic light-wave with a wave-vector $\mathbf{k}$ parallel to the $\mathbf{z}$ axis. Then we can write the electric field

$$\mathbf{E} = E_0(\xi_x \mathbf{x} + \xi_y \mathbf{y})e^{i\omega t}, \tag{B.1}$$

Where ξ_x and ξ_y are complex values and satisfy $|\xi_x|^2 + |\xi_y|^2 = 1$. To describe this field we use the notation

$$\mathbf{E} = E_0 \begin{pmatrix} \xi_x \\ \xi_y \end{pmatrix} e^{i\omega t} \equiv \begin{pmatrix} \xi_x \\ \xi_y \end{pmatrix}. \tag{B.2}$$

We define two orthogonal circular polarization

$$\mathbf{\Sigma}_+ = \begin{pmatrix} -1/\sqrt{2} \\ -i/\sqrt{2} \end{pmatrix} \quad \text{and} \quad \mathbf{\Sigma}_- = \begin{pmatrix} 1/\sqrt{2} \\ -i/\sqrt{2} \end{pmatrix} \tag{B.3}$$

Then we can express any linear polarization

$$\begin{aligned}
\mathbf{E} &= \begin{pmatrix} \cos\theta \\ \sin\theta \end{pmatrix} & \text{(B.4)} \\
&= \frac{1}{\sqrt{2}}[(-\cos\theta + i\sin\theta)\mathbf{\Sigma}_+ + (\cos\theta + i\sin\theta)\mathbf{\Sigma}_-] & \text{(B.5)} \\
&= \frac{1}{\sqrt{2}}[ie^{-i\theta}\mathbf{\Sigma}_+ + e^{i\theta}\mathbf{\Sigma}_-]. & \text{(B.6)}
\end{aligned}$$

B.1.2 Effect of gyrotropic birefringence on a linear polarization

We can now consider the effect of birefringence on a linearly polarized probe described by the quantity

$$\Delta n = \frac{\Delta n_+ - \Delta n_-}{2}, \tag{B.7}$$

which corresponds to a difference in phase shift Φ when crossing the cell

$$\Phi = \Delta n \omega \frac{L}{c}. \tag{B.8}$$

Then

$$\mathbf{E}^{in}_{\text{probe}} = \frac{1}{\sqrt{2}}[ie^{-i\theta}\mathbf{\Sigma}_+ + e^{i\theta}\mathbf{\Sigma}_-] \tag{B.9}$$

becomes after crossing the cell

$$\mathbf{E}^{out}_{\text{probe}} = \frac{1}{\sqrt{2}}[ie^{-i(\theta-\Phi)}\mathbf{\Sigma}_+ + e^{i(\theta-\Phi)}\mathbf{\Sigma}_-]. \tag{B.10}$$

The linearly polarized probe beam then just rotate with an angle $-\Phi$.

B.1.3 Effect of circular dichroism on a linear polarization

So as to describe the effect of circular dichroism on a linearly polarized probe beam, we define the quantities

$$\alpha_m = \frac{\Delta\alpha_+ + \Delta\alpha_-}{2} \quad \text{and} \quad \Delta\alpha = \frac{\Delta\alpha_+ - \Delta\alpha_-}{2}, \tag{B.11}$$

the probe beam $\mathbf{E}^{in}_{\text{probe}}$ then becomes after crossing the cell

$$\mathbf{E}^{out}_{\text{probe}} = \frac{e^{-\alpha_m L}}{\sqrt{2}}[ie^{-i\theta}e^{-\Delta\alpha L}\mathbf{\Sigma}_+ + e^{i\theta}e^{\Delta\alpha L}\mathbf{\Sigma}_-]. \tag{B.12}$$

Assuming that $\Delta\alpha L \ll 1$, we can linearize the expression

$$\mathbf{E}^{out}_{\text{probe}} \simeq e^{-\alpha_m L}[\mathbf{E}^{in}_{\text{probe}} + \frac{\Delta\alpha L}{\sqrt{2}}(-ie^{-i\theta}\mathbf{\Sigma}_+ + e^{i\theta}\mathbf{\Sigma}_-)], \tag{B.13}$$

finally

$$\mathbf{E}^{out}_{\text{probe}} \simeq e^{-\alpha_m L}[\mathbf{E}^{in}_{\text{probe}} + \frac{i\Delta\alpha L}{\sqrt{2}}(ie^{-i(\theta+\pi/2)}\mathbf{\Sigma}_+ + e^{i(\theta+\pi/2)}\mathbf{\Sigma}_-)]. \tag{B.14}$$

The polarization of the probe beam then becomes elliptic with a major axis aligned with the polarization of the incoming probe beam and with a ratio between the minor and the major axis $b/a = \Delta\alpha L$.

B.2 The hydrogen atom in a uniform magnetic field

B.2.1 Hamiltonian of the problem

The hamiltonian of a spinless particle of mass m and charge q subjected simultaneously to a scalar central potential $V(r)$ and a vector potential $\mathbf{A}(\mathbf{r})$ is given by

$$H = \frac{1}{2m}[\mathbf{p} - q\mathbf{A}(\mathbf{r})]^2 + V(\mathbf{r}). \tag{B.15}$$

The potential vector determines the magnetic field $\mathbf{B}(\mathbf{r}) = \nabla \times \mathbf{A}(\mathbf{r})$. When the magnetic field is uniform, the vector potential $\mathbf{A}(\mathbf{r})$ can be written

$$\mathbf{A}(\mathbf{r}) = -\frac{1}{2}\mathbf{r} \times \mathbf{B}. \tag{B.16}$$

After a few algebra [11] we obtain $H = H_0 + H_1 + H_2$ where H_0, H_1 and H_2 are defined by

$$H_0 = \frac{\mathbf{p}^2}{2m} + V(\mathbf{r}) \tag{B.17}$$

$$H_1 = -\frac{\mu_B}{\hbar}\mathbf{L}.\mathbf{B} \tag{B.18}$$

$$H_2 = \frac{q^2\mathbf{B}^2}{8m}\mathbf{R}_\perp^2, \tag{B.19}$$

where $\mu_B = q\hbar/2m$ is the Bohr magneton and the operator $\mathbf{R}_\perp$ is the projection of $\mathbf{R}$ onto a plane perpendicular to $\mathbf{B}$. H_1 and H_2 are respectively called the paramagnetic and the diamagnetic term.

Paramagnetism

The paramagnetic term $H_1 = -\mu_B/\hbar\mathbf{L}.\mathbf{B}$ can be interpreted to be the coupling energy between the magnetic field and the magnetic moment related to the revolution of the electron in its orbit. A simple calculation [11] shows that for an electron, the frequency shift due to the paramagnetic term is 1.40 MHz/gauss.

Diamagnetism

The diamagnetic term describes the coupling between the magnetic field and the magnetic moment induced in the atom. The diamagnetic term is in general negligible relative to the paramagnetic term.

B.2.2 The Zeeman effect

We study in this section the effect of a magnetic field on an optical line of hydrogen which corresponds to the atomic transition between the ground state

1s (n = 1; l = m = 0) and the excited state 2p (n = 2; l = 1; m = +1, 0, -1). We neglect the effect of diamagnetic and then we take $H_0 + H_1$ for the hamiltonian. We choose the Oz axis parallel to **B** then

$$(H_0 + H_1)|nlm> \quad = \quad (H_0 - \frac{\mu_B}{\hbar}BL_z)|nlm> \qquad (\text{B.20})$$

$$= \quad (E_n - m\mu_B B)|nlm>, \qquad (\text{B.21})$$

where $|nlm>$ are the common eigenstates of H_0 (eigenvalue $E_n = -E_I/n^2$), $\mathbf{L}^2$ (eigenvalue $l(l+1)\hbar$) and L_z (eigenvalue $m\hbar$). For the states involved in the resonance line we get

$$(H_0 + H_1)|100> \quad = \quad (H_0 - E_I|100> \qquad (\text{B.22})$$

$$(H_0 + H_1)|21m> \quad = \quad (-E_I/4 - m\mu_B B)|21m> \qquad (\text{B.23})$$

$$= \quad [-E_I + \hbar(\Omega + m\omega_L)]|21m>, \qquad (\text{B.24})$$

where $\Omega = 3E_I/4\hbar$ and $\omega_L = \mu_B B/\hbar$ is the Larmor angular velocity. The excited state is then split into three levels corresponding to the values $m = 1, 0$ and -1 of the magnetic quantum number which corresponds respectively to σ_+, π and σ_- transitions.

B.3 Calculation of the magnetic shielding

B.3.1 Single cylindrical shell in static field

The calculation of the magnetic shielding of the system (See Figure 4.7) is based on a paper of A.G. Mager [16]. The shape which produces the best shielding is the sphere. For a permeability $\mu \gg 1$, a diameter D and a thickness of the wall $d \ll D$, the shielding factor of the spherical sphere is given by

$$S = \frac{4}{3}\frac{\mu d}{D} + 1. \qquad (\text{B.25})$$

For an infinite cylinder with a transversal magnetic field the shielding factor is

$$S_T = \frac{\mu d}{D} + 1. \qquad (\text{B.26})$$

The shielding is always much more effective with transverse field than with longitudinal fields. The calculation of the shielding of the cylindrical shell for longitudinal field is not straightforward. A cylinder with infinite length has no shielding efficiency against static field along its axis. For finite length L, one can obtain an estimation of the shielding factor with an ellipsoid of revolution with the same ratio of length to diameter $m = L/D$. The result of this estimation is

$$S_L = 4NS_T + 1, \qquad (\text{B.27})$$

where $S_T \simeq \mu d/D \gg 1$ is the transverse shielding factor and N is the demagnetization factor. The demagnetization factor for an ellipsoid of revolution has been calculated by Osborn [17] who obtained for $m \gg 1$:

$$N = \frac{1}{m^2}\ln(2m-1). \tag{B.28}$$

For the outer cylinder [1], we obtain $N_o = 0.075$ and $S_L = 25$. For the inner cylinder [2], we obtain $N_i = 0.06$ and $S_L^i = 38.8$.

B.3.2   Double cylindrical shell

Unfortunately, the shielding factor of a shell composed of two concentric cylinders is not the product of the shielding factor of each cylinder calculated separately. Mager gives in his paper [16] an estimation of the resultant longitudinal shielding factor:

$$S_L = 4N_o S_T^o S_T^i \frac{D_m}{L_i + 0.5D_m} \frac{4\Delta D_m}{D_o^2} + 4N_o(S_T^o + S_T^i) + 1. \tag{B.29}$$

Using this estimation, we obtain a longitudinal shielding factor $S_L = 856$ for our system.

B.3.3   Effect of openings

For open-ended cylinders, the field enters the cylinders with an exponential slope. The internal magnetic field is then the sum of this field and the field calculated above. The effect of the openings then decreases the shielding factor. We calculated the shielding factor of our system at the windows of the cell: $S_L^{Total} = 781$.

B.4   Some mathematical objects of quantum mechanics

B.4.1   The density matrix

For a system whose state vector at the instant t is

$$|\psi(t)> = \sum_n c_n(t)|u_n>, \tag{B.30}$$

where $|u_n>$ is an orthonormal basis of the state space, we define the density matrix $\rho(t)$ as

$$\rho(t) = |\psi(t)><\psi(t)|, \tag{B.31}$$

---

[1] $L_o = 200$ mm, $D_o = 50$ mm, $d_o = 5 \times 0.2 = 1$ mm
[2] $L_i = 120$ mm, $D_i = 25$ mm, $d_i = 5 \times 0.2 = 1$ mm

or as

$$\rho_{pn}(t) = c_n^*(t)c_p(t). \tag{B.32}$$

Obviously we have

$$\text{Tr } \rho(t) = 1. \tag{B.33}$$

Let A be an observable, we have the relation

$$< A > (t) = \text{Tr}(\rho(t)A) \tag{B.34}$$

Finally, one can deduce from the Schrödinger equation

$$i\hbar\frac{\mathrm{d}}{\mathrm{d}t}\rho(t) = [H(t), \rho(t)] \tag{B.35}$$

Physical meaning of the density matrix

The term ρ_{nn} represents the average probability of finding the system in the state $|u_n>$, its is called the *population* of the state $|u_n>$. The non-diagonal element ρ_{np} expresses the interference effect between the state $|u_n>$ and $|u_p>$. The non-diagonal terms of the density matrix are called *coherences*.

If the kets $|u_k>$ are eigenvectors of the hamiltonian H with eigenvalues E_k, we obtain from (B.35)

$$\begin{cases} \rho_{nn}(t) = \text{constant} \\ \rho_{np}(t) = e^{\frac{i}{\hbar}(E_p - E_n)t}\rho_{np}(0). \end{cases} \tag{B.36}$$

Bibliography

[1] C. Wieman and T.W. Hänsch, "Doppler-free Laser Polarisation Spectroscopy" (Phy. Rev. Lett., Vol.36, No.20, 1976)

[2] T.W. Hänsch, I.S. Shahin and A.L. Schawlow, "High-Resolution Saturation Spectroscopy of the Sodium D Lines with a Pulsed Tunable Dye Laser" (Phy. Rev. Lett., Vol.27, No.11, 1971)

[3] Eric D. Black, "An introduction to Pound-Drever-Hall laser frequency stabilisation" (Am. J. Phys., Vol. 69, No.1, 2001)

[4] Gary C. Bjorklund, "Frequency-modulation spectroscopy: a new method for measuring weak absorptions and dispersions" (Optics Letters, Vol.5, No.1, 1980)

[5] Y. Yoshikawa & al.,"Frequency stabilization of a laser diode with use of light-induced birefringence in an atomic vapor" (Applied Optics, Vol.42, No. 33, 2003)

[6] T. Petelski & al., "Doppler-free spectroscopy using magnetically induced dichroism of atomic vapor: a new scheme for laser frequency locking" (Eur. Phys. J. D 22, 2003)

[7] H. Kogelnik and T. Li, "Laser Beams and Resonators" (Applied Optics / Vol.5, No.10 / October 1966)

[8] T. Klaassen, "Imperfect Fabry-Pérot resonators" (Thesis , Universiteit Leiden, 2006)

[9] Andrej Cadez, "Internal scattering in Fabry-Pérot cavities" (Phys. Rev., Vol.41 N.11, 1990)

[10] L. G. Gouy, "Sur une propriete nouvelle des ondes lumineuses" (Compte-Rendu Acad. Sci. Paris, vol. 110, pp. 1251-1253, 1890)

[11] C. Cohen-Tannoudji, B. Diu and F. Laloë, "Quantum Mechanics" (Wiley, 1977)

[12] M. Born and E. Wolf, "Principles of Optics" (Pergamon Press, 1975)

[13] Antony E. Siegman, "Lasers" (Stanford University, 1986)

[14] Rodney Loudon, "The quantum theory of light" (Oxford, 1973)

[15] Jook Walraven, Lectures notes

[16] A.J. Mager, "Magnetic Shields" (IEEE Transactions on Magnetics, Vol.6, No.1, 1970)

[17] J.A. Osborn, "Demagnetizing factor of the general ellipsoid" (Phy. Rev.,Vol.67, No.11-12, 1945)